Numerical Analysis of Asymmetric Differential Inductors

Masaki Kanemaru, Daisuke Imanishi, Kenichi Okada, and Akira Matsuzawa
Department of Physical Electronics, Tokyo Institute of Technology
kanemaru@ssc.pe.titech.ac.jp

Introduction

Due to miniaturization of CMOS process, many kinds of commercial radio ICs have been realized by Si CMOS. On the other hand, it has become a difficult challenge to characterize on-chip inductors because of eddy-current loss caused by Si substrate, and use of inaccurate models might involve degradation of circuit performance. Thus, accurate modeling of on-chip inductors is a very important issue in high-frequency circuit design [1].

This paper reports a new method for numerical analysis of symmetric differential inductors. Ideality of symmetric differential inductors is an important factor to design differential circuits. As previous work, asymmetry can not be evaluated accurately. In [2], difference between Y_{11} and Y_{22} is used to estimate asymmetric properties of differential inductors. However, the difference is involved in only difference in shunt parasitic components. In [1], three-port modeling of differential inductors is presented. A 2-π-shape equivalent circuit model is employed in [1], and each circuit parameter is extracted by numerical optimization. Therefore, left-right asymmetry can not be evaluated accurately by the method in [1]. In this work, the matrix-decomposition technique is employed [3]. Left- and right-half inductances can be calculated by 3-port S-parameters as well as mutual inductance.

Asymmetry of on-chip differential inductors is often caused by a surrounded ground loop, which is sometimes unavoidable due to requirement of layout shrinking. This paper also presents simulated and measured results for analyzing the asymmetric ground loop as an application of the matrix-decomposition technique, which are applied to 1-, 2-, and 3-turn of symmetric inductors.

Matrix-Decomposition Technique

In this section, the matrix-decomposition technique [3] and its application to the analysis of differential inductors are explained.

A. Derivation of matrix $\mathbf{Y}_c$

Figure 1(a) shows an equivalent circuit of differential inductors, which consists of core, shunt, and lead parts [4], [5]. The core part expresses self and mutual inductances with parasitic resistance and capacitance, which are characterized by z_n. The core part is also expressed by a matrix $\boldsymbol{Y}_c$. The shunt part characterizes ILD and Si substrate, and it is expressed by a matrix $\boldsymbol{Y}_{sub}$. The lead part characterizes lead lines, which are parasitic components here. The lead part is also expressed by matrix $\boldsymbol{Y}_{open}$ and $\boldsymbol{Z}_{short}$. These matrices can be combined by the following equations.

$$\mathbf{Z}_{meas'} = (\mathbf{Y}_{meas} - \mathbf{Y}_{open})^{-1} - (\mathbf{Z}_{short}{}^{-1} - \mathbf{Y}_{open})^{-1}, \quad (1)$$

$$\mathbf{Y}_{meas'} = \mathbf{Y}_c + \mathbf{Y}_{sub}, \quad (2)$$

where admittance matrix $\boldsymbol{Y}_{meas}$ is converted from measured S-parameter. To decompose each part of multi-port inductor in Fig. 1(a), first the matrix $\boldsymbol{Y}_{sub}$ is calculated. The matrix $\boldsymbol{Y}_{sub}$ can be expressed by admittances y_{subn} as follows.

$$\mathbf{Y}_{\mathrm{sub}} = \begin{pmatrix} y_{\mathrm{sub1}} & 0 & 0 \\ 0 & y_{\mathrm{sub2}} & 0 \\ 0 & 0 & y_{\mathrm{sub3}} \end{pmatrix} \tag{3}$$

When $v_a = v_1 = v_2 = v_3$, no current flows into z_n shown in Fig. 1. Here, v_a is arbitrary number. The following equation is derived from Eqs.(2)

$$\begin{pmatrix} i_1 \\ i_2 \\ i_3 \end{pmatrix} = \mathbf{Y}_{\mathrm{meas'}} \begin{pmatrix} v_a \\ v_a \\ v_a \end{pmatrix} = (\mathbf{Y}_c + \mathbf{Y}_{\mathrm{sub}}) \begin{pmatrix} v_a \\ v_a \\ v_a \end{pmatrix} = \mathbf{Y}_{\mathrm{sub}} \begin{pmatrix} v_a \\ v_a \\ v_a \end{pmatrix} \qquad \left[\because \mathbf{Y}_c \begin{pmatrix} v_a \\ v_a \\ v_a \end{pmatrix} = 0 \right] \tag{4}$$

Therefore, each $y_{\mathrm{sub}n}$ in $\boldsymbol{Y}_{\mathrm{sub}}$ can be calculated by the following equation.

$$y_{\mathrm{sub}n} = \sum_{i=1}^{3} y_{\mathrm{meas'}\,\mathrm{ni}} \tag{5}$$

B. Conversion of matrix Y_c to Z_{core}

Figure 2 shows the core part of the entire equivalent circuit in Fig. 1, which is expressed by the matrix $\boldsymbol{Y}_c$.

$$\mathbf{i} = \begin{pmatrix} i_1 \\ i_2 \\ i_3 \end{pmatrix} = \mathbf{Y}_c \begin{pmatrix} v_1 \\ v_2 \\ v_3 \end{pmatrix} = \mathbf{Y}_c \mathbf{v} \tag{6}$$

In this case, we need each parameter of z_n and M_{nm}, so the matrix $\boldsymbol{Y}_c$ is converted into an impedance matrix $\boldsymbol{Z}_{\mathrm{core}}$. The matrix $\boldsymbol{Z}_{\mathrm{core}}$ is defined by the following equations.

$$\mathbf{v}_z = \begin{pmatrix} v_{z1} \\ v_{z2} \end{pmatrix} = \begin{pmatrix} z_1 & -j\omega M_{12} \\ -j\omega M_{21} & z_2 \end{pmatrix} \begin{pmatrix} i_{z1} \\ i_{z2} \end{pmatrix} = \mathbf{Z}_{\mathrm{core}} \mathbf{i}_z , \tag{7}$$

where vectors $\boldsymbol{v}$, $\boldsymbol{i}$, $\boldsymbol{v}_z$, and $\boldsymbol{i}_z$ are defined as shown in Fig. 1(b). Each element of the matrix $\boldsymbol{Z}_{\mathrm{core}}$ expresses self and mutual components directly. In this case, M_{21} is equal to M_{12}. Here, current direction of i_{z2} is opposite to i_{z1} while they have the same direction in the original matrix-decomposition technique [3]. It is because error sensitivity of port 2 is larger than the others, and current direction is symmetrically defined as shown in Fig. 1(b) to avoid asymmetric error in measurements.

$\boldsymbol{Z}_{\mathrm{core}}$ can be derived from $\boldsymbol{Y}_c$. Rank of the matrix $\boldsymbol{Z}_{\mathrm{core}}$ is 2, and the matrix $\boldsymbol{Y}_c$ consists of the same components as shown in Fig. 1(b). Thus, rank of $\boldsymbol{Y}_c$ is also 2 although $\boldsymbol{Y}_c$ is a 3×3 matrix. The matrix $\boldsymbol{Y}_c$ is not a regular matrix, and it does not have an inverse matrix. In this work, converting matrices $\boldsymbol{A}$ and $\boldsymbol{B}$ are utilized, which are also not a regular matrix.

The converting matrices $\boldsymbol{A}$ and $\boldsymbol{B}$ are derived by the following procedure. Vectors $\boldsymbol{i}$ and $\boldsymbol{v}$ are converted into vectors $\boldsymbol{i}_z$ and $\boldsymbol{v}_z$ by the following equations.

$$\mathbf{v}_z = \begin{pmatrix} v_{z1} \\ v_{z2} \end{pmatrix} = \begin{pmatrix} v_1 - v_3 \\ v_2 - v_3 \end{pmatrix} = \mathbf{A}\mathbf{v} , \quad \mathbf{i}_z = \begin{pmatrix} i_{z1} \\ i_{z2} \end{pmatrix} = \begin{pmatrix} i_1 \\ i_2 \end{pmatrix} = \mathbf{B}\mathbf{i} \tag{8}$$

$$\mathbf{A} = \begin{pmatrix} 1 & 0 & -1 \\ 1 & -1 & 0 \end{pmatrix} \tag{9}$$

Here, $i_1 + i_2 + i_3$ is equal to 0 as shown in Fig. 1(b), so i_2 in Eq. (8) is also expressed by $-i_1$-i_3 as an example. Thus, matrix $\boldsymbol{B}$ has four solutions. However, the first one is better from the view point of error sensitivity.

$$\mathbf{B} = \begin{pmatrix} 1 & 0 & 0 \\ 0 & 1 & 0 \end{pmatrix}, \begin{pmatrix} 1 & 0 & 0 \\ -1 & 0 & -1 \end{pmatrix}, \begin{pmatrix} 0 & -1 & -1 \\ 0 & 1 & 0 \end{pmatrix}, \begin{pmatrix} 0 & -1 & -1 \\ -1 & 0 & -1 \end{pmatrix} \tag{10}$$

Eqs. (6)(8)(9) are substituted into Eq. (7), and the following equations are obtained.

$$\mathbf{A} = \mathbf{Z}_{\text{core}}\mathbf{B}\mathbf{Y}_{\text{c}} \tag{11}$$

Matrices $\boldsymbol{A}$ and $\boldsymbol{B}$ are not regular matrix. Matrix $\boldsymbol{Z}_{\text{core}}$ is 2×2 matrix. $\boldsymbol{Y}_{\text{c}}$ is shrunk to $\boldsymbol{Z}_{\text{core}}$ by pseudo-inverse matrix $\boldsymbol{A}^{+}$. For example, $\boldsymbol{A}^{+}$ can be defined as follows.

$$\mathbf{A}^{+} = \mathbf{B}^{\text{T}} \tag{12}$$

$$\mathbf{A}\mathbf{A}^{+} = \begin{pmatrix} 1 & 0 & -1 \\ 0 & 1 & -1 \end{pmatrix}\begin{pmatrix} 1 & 0 \\ 0 & 1 \\ 0 & 0 \end{pmatrix} = \mathbf{I} \tag{13}$$

Finally, the following equations are derived. $\boldsymbol{Z}_{\text{core}}$ is expressed by Eq. (14). The self and mutual inductances are calculated from the measured S-parameter.

$$\mathbf{Z}_{\text{core}} = (\mathbf{B}\mathbf{Y}_{\text{c}}\mathbf{A}^{+})^{-1} \tag{14}$$

Simulation and Experimental Results

In this section, the proposed method is performed for simulation and measurement results. Figure 2 shows a simulation model to evaluate the asymmetric ground loop. The asymmetry is realized by moving the left-side ground plane as shown in Fig.2. $\text{Im}[z_1]/\omega$ and $\text{Im}[z_2]/\omega$ are utilized to evaluate left-right asymmetry. Figure 3 plots the mismatch between left- and right-half inductances as a function of Δx. The mismatch of 2-turn symmetric inductor is smaller than 1- and 3-turn. When the number of turn is even, left- and right-half components are equally influenced by surrounding layout. Thus, the mismatch between left- and right-half inductances is canceled. Next, measurement results are shown. Figure 4 shows microphotographs of differential inductors. Figure 4(a) shows ideal one, which has a symmetric structure except for the under path at the cross-point. Figure 5 shows inductances derived from measured S-parameters with the proposed method. Figure 5(a) shows inductances of the ideal structure, and there is no large difference in the inductances. In Fig. 4(b), left side ground plane is closer to the spiral part, and 4% mismatch exists as shown in Fig. 5(b).

Conclusions

In this paper, the numerical analysis using the matrix-decomposition technique is proposed to evaluate left-right asymmetry in differential inductors. Both left- and right-half components can be calculated by the analythical equations without parameter extraction using numerical optimization, so difference between the components can be accurately evaluated.

References

[1] K. Okada, *et al*., *EuMC*, Oct. 2007, pp. 520– 523.
[2] Y. Aoki, *et al.*, *EuMC*, Oct. 2007, pp. 339–342.
[3] T. Ito, *et al.*, ARFTG, June 2007, pp. 212–215.
[4] J. R. Long, *et al*., *JSSC*, vol. 32, no. 3, pp. 357–369, Mar. 1997.
[5] A. M. Niknejad, *et al*., *JSSC*, vol. 33, no. 10, pp. 1470–1481, Oct. 1998.

Figures

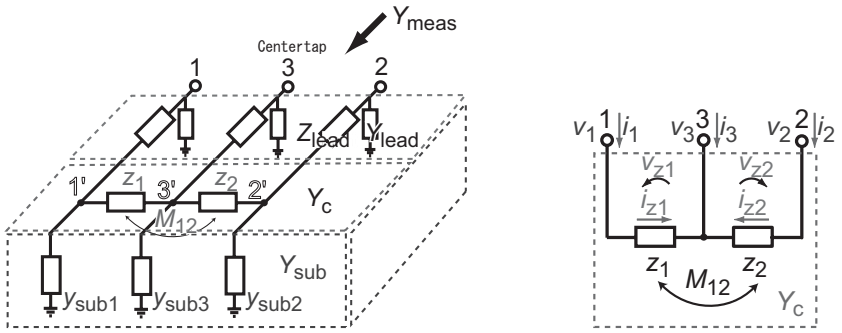

(a) expressed core, shunt, and lead parts (b)core part

Figure 1. Equivalent circuit of a differential inductor.

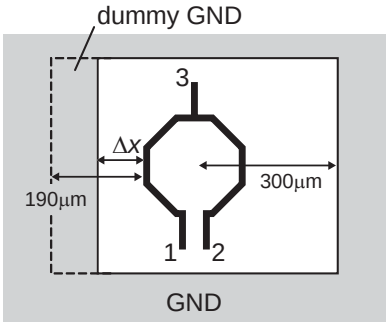

Figure 2. Simulation model.

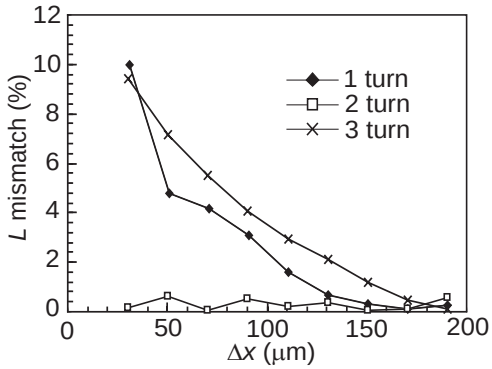

Figure 3. The mismatch between left- and right-half inductances.

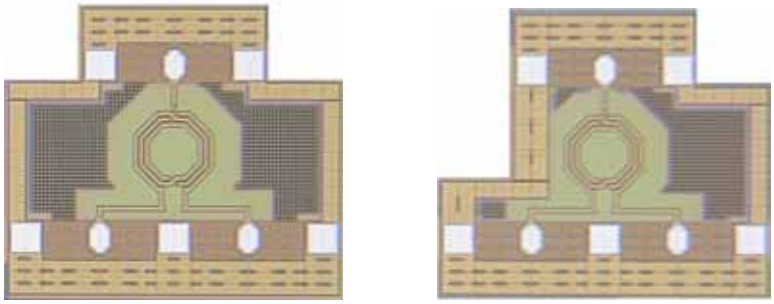

(a) ideal (b) asymmetric

Figure 4. Micrograph.

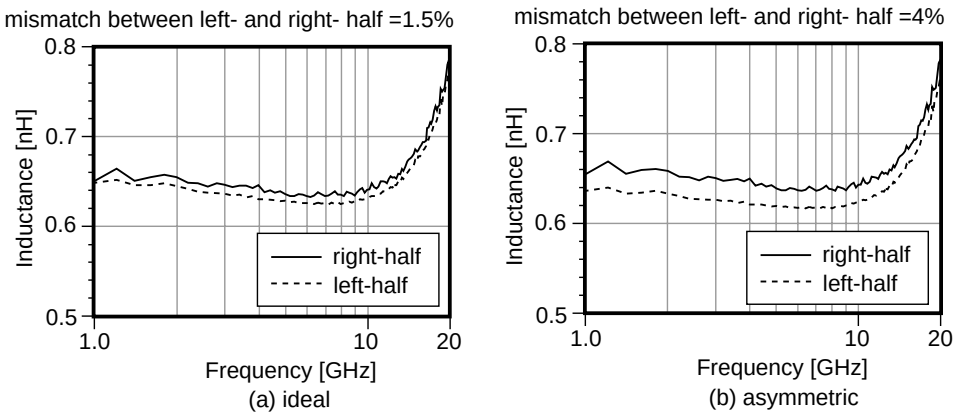

Figure 5. Left- and right-half inductance derived from measurement.